RSC Advances

PAPER

View Article Online
View Journal | View Issue

Cite this: *RSC Adv.*, 2024, **14**, 13142

Antioxidant-rich brilliant polymeric nanocomposites for quick and efficient non-enzymatic hydrogen peroxide sensor†

M. S. Hashem, *[a] Hend S. Magar,[b] Asmaa M. Fahim[c] and Rokaya A. Sobh[a]

In our current research, a new type of functional nanocomposites known as poly(methyl methacrylate/*N*,*N*-dimethyl aminoethylmethacrylate/(*E*)-2-cyano-*N*-cyclohexyl-3 (dimethylamino) acrylamide) [poly(MMA/DMAEMA/CHAA)] has been developed. These nanocomposites were created using microemulsion polymerization in conjunction with synthesized titanium dioxide (TiO_2), and vanadium pentoxide (V_2O_5) nanoparticles. To understand the physio-chemical characteristics of the poly(MMA/DMAEMA/CHAA) and the metal oxide nanoparticles (MOs) integrated within them, various analytical techniques were employed. These techniques included Fourier-transform infrared spectroscopy (FT-IR), proton nuclear magnetic resonance (^{1}H NMR), X-ray diffraction analysis (XRD), thermogravimetric analysis (TGA), scanning electron microscopy (SEM), energy dispersive X-ray spectroscopy (EDX), transmission electron microscopy (TEM), and electrical approaches such as cyclic voltammetry (CV) and electrical impedance spectra (EIS). Based on the TEM results, nanospheres with a well-defined structure were developed for both the pure polymer and its composite with sizes ranging from 45 to 75 nm. All the TiO_2 and V_2O_5-based nanocomposites showed significantly enhanced electrical attributes, with capacitance values surpassing those of the poly(MMA/DMAEMA/CHAA) nanosphere assemblies by a considerable margin. As a result, both direct electron transfer and direct hydrogen peroxide identification were evaluated for the nanocomposites. The amperometry results demonstrated a lower detection limit of 0.0085 μM and a rapid linear sensitivity in the range of 1 to 800 μM. The greatly improved electrolytic qualities of these nanocomposites make them suitable for various applications in fields such as battery storage, sensors, and biosensors.

Received 7th March 2024
Accepted 15th April 2024

DOI: 10.1039/d4ra01768d

rsc.li/rsc-advances

1. Introduction

Polymers are a diverse group of materials that have gained significant attention due to their wide range of physico-chemical properties, highly valued in numerous applications.[1] One key reason for their current popularity is their ability to undergo reversible and irreversible changes in response to external stimuli, such as bioactive substances, electrical or magnetic fields, light irradiation, pH, specific ions, temperature, and more. Polymers can be fashioned into various forms, including films, gels,[2] solids,[3] solutions, or nanoparticles.[4] By carefully modifying or synthesizing specific materials, it is possible to develop customized sensing devices for specific tasks.[5] Amorphous poly methyl methacrylate (PMMA) is a member of the acrylate family, known for its excellent optical qualities. Moreover, it has the capability to interact with metal nanoparticles, thereby enhancing their material properties.[6] Solubility, mechanical strength, and optical characteristics are among those that could be enhanced.

Hydrogen peroxide (H_2O_2) plays a crucial role in various industries including biology, medicine, and food, making the quick and accurate determination of its presence essential.[7] Several analytical methods such as chemiluminescence,[8] spectroscopy,[9] and titrimetric analysis, have been utilized for this purpose. However, these methods are expensive, time-consuming, lack sensitivity and can be affected by other substances in the samples being analyzed. To overcome these limitations, electrochemical sensors based on nanomaterials show promise.[10–12] Electrochemical sensors and biosensors achieve all promising features as ideal tools for sensitive analysis of chemicals in biological and environmental samples,[13–15] accurate diseases diagnosis and fast analyte detection. All these interesting properties of the sensors are basically dependent on the electrode surface materials. Therefore, the modification of the electrode surface with a new

[a]*Polymers and Pigments Department, National Research Centre, Dokki, P.O. Box 12622 Giza, Egypt. E-mail: ms.hashem@nrc.sci.eg*

[b]*Applied Organic Chemistry Department, National Research Centre, Dokki, P.O. Box 12622 Giza, Egypt*

[c]*Department of Green Chemistry, National Research Centre, Dokki, P.O. Box 12622 Giza, Egypt*

† Electronic supplementary information (ESI) available. See DOI: https://doi.org/10.1039/d4ra01768d

nanomaterial (such as polymer-based nanocomposites)[16] is important to perform an effective electrochemical sensor platform. Functional groups of polymers could attach to metal oxide nanoparticles, resulting in strong adhesion of the nanoparticles to the electrode surface and chemical durability.[17] These metal oxides have electrocatalytic activity properties which enhance the electrochemical properties of the polymer.

The recent study focuses on facile synthesis, full characterization and potential applications and electrochemical features of a new nanocomposite made of poly(MMA/DMAEMA/CHAA) and metal oxides. However, there are no existing studies on electrodes modified with poly(MMA/DMAEMA/CHAA) that can be utilized for non-enzymatic H_2O_2 detection sensor. The poly(MMA/DMAEMA/CHAA)-TiO_2 nanocomposite shows promising enhancements in electrochemical properties, making it an intriguing candidate for investigating its potential application in hydrogen peroxide detection, energy storage, and sensors.

2. Experimental

2.1. Materials and instrumental analysis

N,*N*-Dimethylaminoethyl methacrylate (DMAEMA, 99%) was purchased from Fluka Chemie (Buchi, Switzerland) and purified by distillation under vacuum (69–70, 1–2 mmHg) before use. Methyl methacrylate (MMA, 99%) was obtained from Merck Schuchardt OHG (Hohenbrun, Germany) purified using a column with basic alumina and stored at 4 °C until use. (*E*)-2-Cyano-*N*-cyclohexyl-3-(dimethylamino)acrylamide (CHAA, ≥99.9%) was previously synthesized and characterized as a novel monomer.[18] Polyvinylpyrrolidone (PVP-40, >99%) was from Bio Basic Canada INC (Ontario, Canada). Ammonium persulfate (APS, ≥98%) was obtained from BDH Laboratory Supplies (Poole, England), and sulfuric acid (H_2SO_4, 98%) from Loba-Chemie PVT-LTD (Mumbai, India). Hydrogen peroxide (H_2O_2, 30%), hydrochloric acid (HCl, 37%), ammonium hydroxide solution (NH_4OH, 30%), dimethyl sulfoxide (DMSO, ≥99.9%) sodium metavanadate ($NaVO_3$, ≥98%), cetyltrimethylammonium bromide ($(N(CH_3)_3)Br$, ≥99%), titanium tetra chloride ($TiCl_4$, 99.9%), glycerol (≥99%), potassium ferricyanide ($C_6N_6FeK_3$, 99%), potassium ferrocyanide ($K_4Fe(CN)_6$, 99.5%), potassium dihydrogen phosphate (KH_2PO_4, 99%), potassium monohydrogen phosphate (K_2HPO_4, 99%), potassium chloride (KCl, 99%), and sodium hydroxide pellets (NaOH, ≥98%) were provided by Sigma-Aldrich Chemie GmbH (Steinheim, Germany).

The Shimadzu 8101 FT-IR spectrometer was utilized to analyze the chemical bonding of prepared samples within the range of 400 to 4000 cm^{-1}. X-Ray powder diffraction (XRD) analysis was conducted using a Philips X-Pert model with a Cu Kα radiation source, covering the 2θ range from 20 to 80°. The particle size of nanocomposites was determined through transmission electron microscopy (TEM, model JEOL JEM-2100). Scanning electron microscope (SEM) and energy dispersive X-ray spectroscopy (EDX) studies were carried out with the JEOL-JSM-6390LV. Thermal gravimetric analysis (TGA model Shimadzu TGA-50) was performed at temperatures ranging from 30 to 1000 °C, with weight loss measured at a heat flow rate of 10 °C min^{-1} in the presence of nitrogen. Electrochemical characterizations were carried out using a CHI 660 potentiostat, the cyclic voltammetry (CV), and electrochemical impedance spectroscopy (EIS) were performed in three replications using a 5 mM $[Fe(CN)^6]^{3-/4-}$ (1 : 1) redox probe containing 0.1 M KCl solution as a supporting electrolyte. CV measurements involved cycling the potential between −0.4 to +0.7 V with a scan rate of 50 mV s^{-1}. Impedimetric evaluation was carried out with frequencies ranging from 10 000 to 0.1 Hz at open circuit potential under a 10 mV AC-potential amplitude. To assess the individual resistance of the electrochemical system, impedance data were fitted to an equivalent circuit (Randles) model. All electrochemical tests were performed at room temperature (25 ± 2 °C).

2.2. Synthesis of metal oxides nanoparticles

For V_2O_5 synthesis, dissolve sodium metavanadate (0.1 g) in 100 ml double distilled. 1.2 g of ammonium chloride was added to the above solution with vigorous stirring at room temperature to dissolve completely. The color of the solution changed to orange color after a few minutes of stirring. Cetyltrimethylammonium bromide (0.5 g) was added to the last solution with increasing the temperature to 80 °C. The solution color changed to dark brown color and the pH of the solution in the range between 6 and 8 during the reaction. After 1 hour, the color of the solution changed to yellow color. The suspension solution evaporated and calcined at 600 °C for 4 hours. The synthesis of TiO_2 was prepared by the following method: A solution of 18.0 ml of titanium tetra chloride ($TiCl_4$, 0.1 M) was dropped to aqueous solution of glycerol (50 ml) in ice water bath (5 °C) with vigorous stirring. 2.5 M of ammonium hydroxide solution (300 ml) added to the above solution to produce titanium hydroxide ($Ti(OH)_2$) precipitate. The product was washed several times with double distilled water (DDW) and collected by centrifugation and left to dry at 80 °C. The dried compound was calcinated for 2 hours at 300 °C to produce TiO_2 nanoparticles.

2.3. Synthesis of poly(MMA/DMAEMA/CHAA) nanospheres

Microemulsion technique was used to prepare poly(MMA/DMAEMA/CHAA) nanospheres. A three-neck round bottom flask with a nitrogen inlet, condenser, water bath, and heating plate with a magnetic stirrer was used in the experiment. Separately, 0.5 g of PVP as an emulsifier and 0.25 g of APS as an initiator were dissolved in 5 ml of DDW. First, the reaction mixture (emulsifier and 10% initiator solution) was purged with N_2 at 65 °C for 30 minutes. Second, when the temperature is kept constant, the monomers MMA, DMAEMA, and CHAA (3 : 2 : 1) slowly dropped along but separate from the retained initiator solution. After 15–20 minutes, a bluish color appeared, indicating polymerization and the reaction was allowed to proceed at 70 °C for 4 hours. The resulting polymer was repeatedly washed with ethanol and DDW to eliminate homopolymers and unreacted monomers before drying at 50 °

Fig. 1 Synthesis of poly(MMA/DMAEMA/CHAA) nanospheres and nanocomposites *via* microemulsion polymerization and poly(MMA/DMAEMA/CHAA)-MOs screen-printed electrode modification method with their electrochemical measurements.

C for characterization. Fig. 1 shows a schematic representation of the poly(MMA/DMAEMA/CHAA) nanospheres synthesis.

2.4. Synthesis of poly(MMA/DMAEMA/CHAA)-MO nanocomposites

Microemulsion polymerization was used to produce poly(MMA/DMAEMA/CHAA) nanocomposite materials containing metal oxide nanoparticles. Independently, TiO_2 and V_2O_5 nanoparticles metal oxides (MOs) were dispersed in MMA, DMAEMA, and CHAA by sonication for 15 min. The polymerization processes of individual metal nanoparticles were performed as described in the previous section. The synthesis scheme of the poly(MMA/DMAEMA/CHAA)-MOs nanocomposite materials is explained in Fig. 1.

2.5. Viscometrical molecular weight measurement

Viscometrical measurements were conducted using an Ubbelohde Capillary Viscometer type 531/10I to determine the viscosity-average molecular weight. By utilizing the experimental viscosity of the polymer solutions at three different concentrations, intrinsic viscosity and viscometrical molecular weight were determined. Several formulas for calculating the intrinsic viscosity of diluted polymer solutions have been presented. These methods can be useful when many samples need quick examination and beneficial in industrial laboratories due to their efficiency. The most practical formula is the Solomon-Ciute (SC, eqn (1)) method.[19,20]

$$[\eta] = [2(\eta_{sp} - \ln \eta_r)^{\frac{1}{2}}]/C \quad (1)$$

where C is mass concentration, $\eta_{sp} = \eta_r - 1$ is specific viscosity, $\eta_r = t/t_0$ is relative viscosity (where t is time of solution and t_0 is time of follow of pure solvent), and η = intrinsic viscosity.

Respective to Huggins equation, the value of intrinsic viscosity changes with the molecular weight of the polymer in a solvent.

$$[\eta] = KM^{\alpha} \quad (2)$$

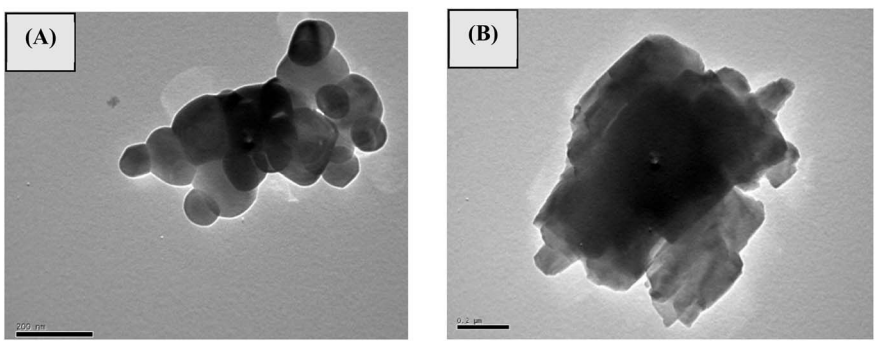

Fig. 2 TEM images of (A) TiO_2 and (B) V_2O_5 nanoparticles.

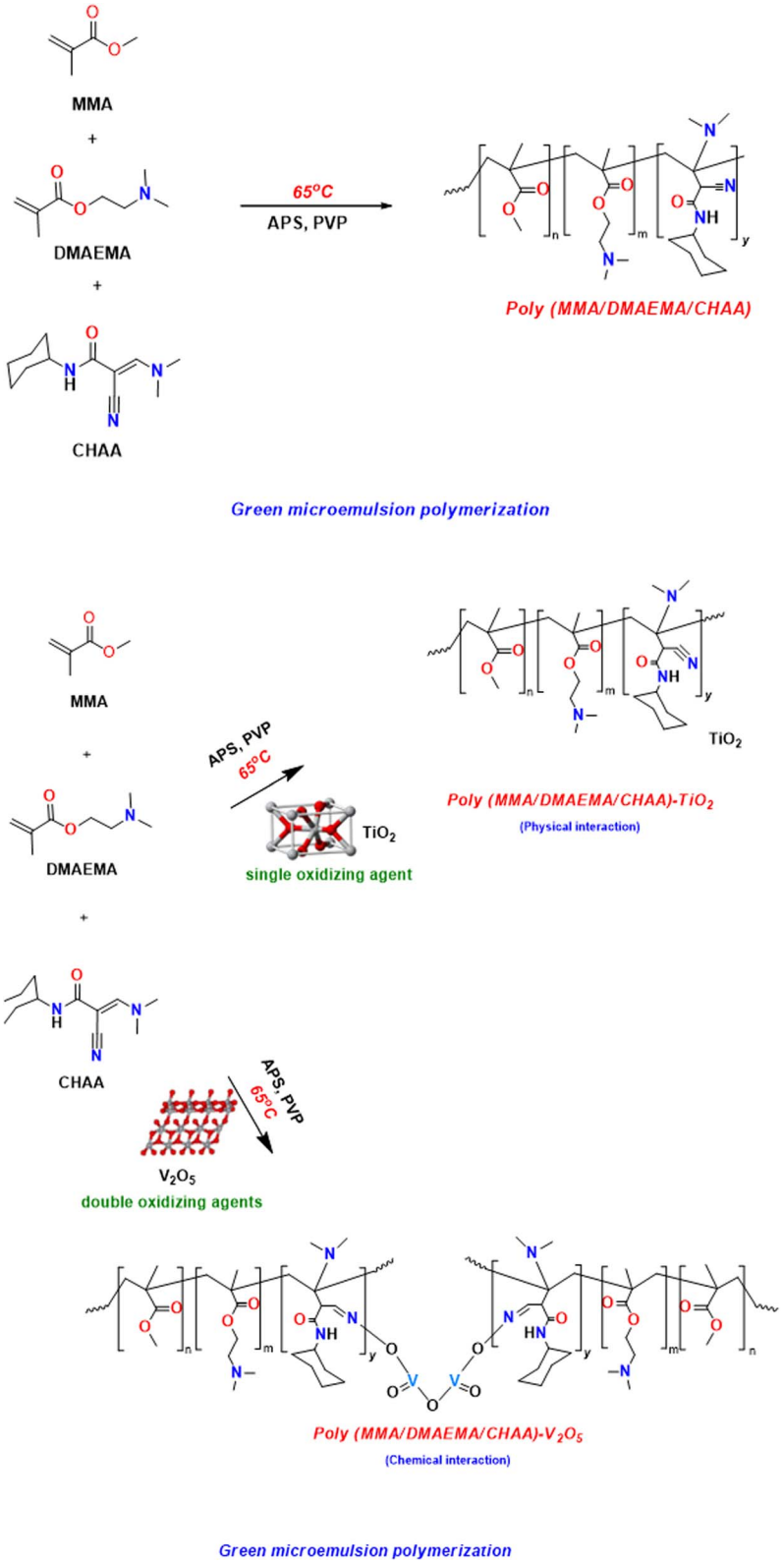

Fig. 3 Synthesis of poly(MMA/DMAEMA/CHAA) nanospheres and nanocomposites.

where K and α are constants for a given polymer–solvent-temperature system. These constants are determined according to eqn (3) by evaluating a plot of $\log[\eta]$ *versus* log molecular weight.[21,22]

$$\log[\eta] = \log K + a \log M \quad (3)$$

2.6. Antioxidant activities

To assess the scavenging activity of various heterocyclic compounds, we utilized the DPPH (2,2-diphenyl-1-picrylhydrazyl) free radical.[23] In this experiment, a 100 μM DPPH solution in methanol was mixed with equal volumes of different concentrations of the test compounds (0–200 μM ml^{-1}) in methanol, and the mixture was thoroughly combined. The reaction mixture was then left to incubate in the dark at room temperature for 30 minutes and subsequently measured at 520 nm. By plotting the percentage of $DPPH^{\cdot}$ scavenging against concentration, we created a standard curve, and the percentage of scavenging was calculated using the following equation:

$$\% \text{ scavenging} = [(\text{absorbance of blank} - \text{absorbance of test})/\text{absorbance of blank}] \times 100$$

IC_{50} was obtained from a plot between the concentration of test compounds and % scavenging. Ascorbic acid (vitamin C) was used as a standard for comparison.

2.7. Fabrication of modified electrodes for sensing applications

5.0 mg of prepared nanocomposites were dispersed in 1.0 ml of distilled water, followed by ultrasonic treatment for 60 minutes to achieve an appropriate suspension. Then, 30 μl of different dispersions were individually drop-casted onto the working electrode surface of the screen-printed electrodes (SPEs). Fig. 1 demonstrates the fabrication steps of SPS modification with the nanomaterials. The electrochemical activities of each modified SPE were tested in 0.1 M of KCl supporting electrolyte containing 5 mM of potassium ferricyanide/potassium ferrocyanide ($[Fe(CN)_6]^{3-/4-}$), as the

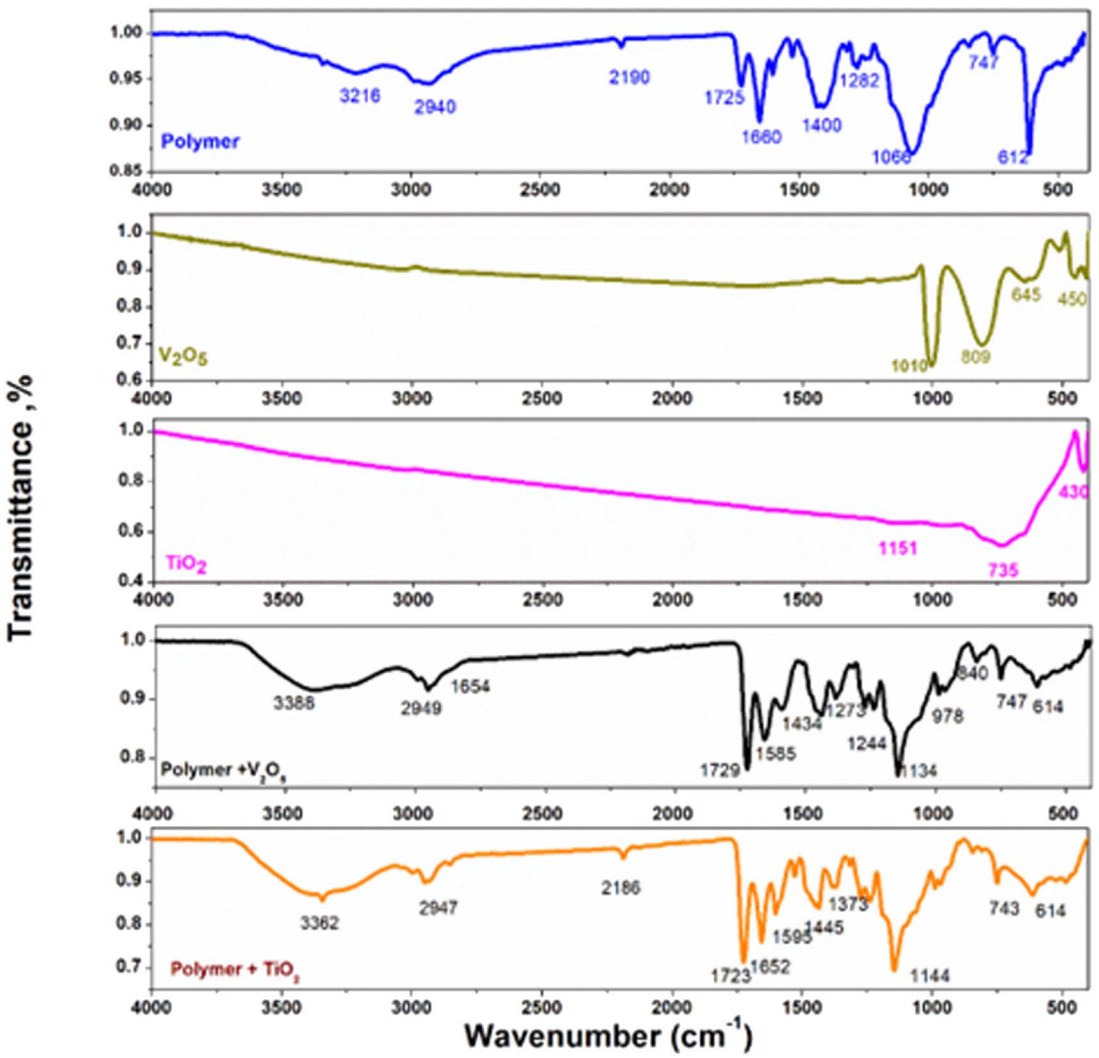

Fig. 4 FTIR spectra of V_2O_5, TiO_2, poly(MMA/DMAEMA/CHAA), poly(MMA/DMAEMA/CHAA)-V_2O_5, and poly(MMA/DMAEMA/CHAA)-TiO_2.

standard redox probe. Both CV and EIS data were collected for each modified electrode, and their electrochemical performance was compared with the un-modified electrode, serving as the negative control.

3. Results and discussion

3.1. Synthesis of metal oxides (MOs) nanomaterials

In this study, TiO_2 and V_2O_5 nanomaterials were successfully prepared, and their nanoscale sizes were confirmed by TEM, as shown in Fig. 2. The TEM results reveal that the size of TiO_2 nanoparticles ranges from 20 to 40 nm in diameter (Fig. 2A), while the diameter of the V_2O_5 nano sheets ranges from 5 to 10 nm (Fig. 2B).

3.2. Characterization of polymeric nanospheres and nanocomposites

Microemulsion polymerization can be used to create innovative, versatile polymeric nanospheres, and a semi-transparent, uniformly distributed, and thermodynamically stable[24,25] poly(MMA/DMAEMA/CHAA) nanospheres was generated with a solid content of 15.5% and a monomer conversion of 92%, as displayed in Fig. 3. So, at the breakdown temperature of the APS initiator, the monomer mixture of MMA, DMAEMA, and CHAA was gradually added to the aqueous emulsifier solution.[26,27] Additionally, with high yield, the poly(MMA/DMAEMA/CHAA)-MOs was quickly produced as a homogenous and semi-transparent copolymer latex. Pure poly(MMA/DMAEMA/CHAA) nanospheres and TiO_2 and V_2O_5-based nanocomposites were produced and investigated by FT-IR, H^1 NMR, SEM, EDX, TEM, and TGA; in addition, the electrochemical properties were studied. In the case of the nanocomposite formation containing the V_2O_5 particles, the V_2O_5 acts with APS as double oxidizing agents for the free radical polymerization process.

3.2.1. Molecular weight determination. An Unbeholden Capillary Viscometer type 531/10I was used to measure the intrinsic viscosity and viscometry molecular weight. Initially, a solution of poly(MMA/DMAEMA/CHAA) was prepared in DMSO at three varying concentrations: 0.001, 0.002, and 0.004 g ml^{-1}. Subsequently, the flow time of the solutions through the Capillary Viscometer was recorded at room temperature. Lastly, the experimental viscosity of the polymer solutions at the three distinct concentrations was calculated by substituting values into eqn (1) and (2). The calculated viscometry molecular weight for poly(MMA/DMAEMA/CHAA) was approximately 303 521 g $mol^{-1} \pm 23\,725$.

3.2.2. FT-IR analysis. The composition of the synthesized nanoparticles, polymeric nanospheres, and the constructed nanocomposites was characterized by FT-IR analysis in the wavenumber ranging between 400 and 4000 cm^{-1} as observed in Fig. 4. In synthesized V_2O_5 nano-sheets, the V=O vibrations band appears at 1009 cm^{-1}, for V–O–V asymmetric and symmetric stretch band appear at 808 cm^{-1} and 450 cm^{-1}, respectively.[28–30] For TiO_2 nanoparticles, the symmetry and asymmetric stretching vibration of water molecule OH groups appeared in wide band range at 3800–3000 cm^{-1} which produced according to the adsorption of water on TiO_2 surface. The bending hydroxyl group of Ti–O–H band appears at 1150 cm^{-1}, and the peak which found at 3015 cm^{-1} is corresponding to the free hydroxyl group. Additionally, the TiO_2 nanoparticles stretching vibrational modes presented at 753

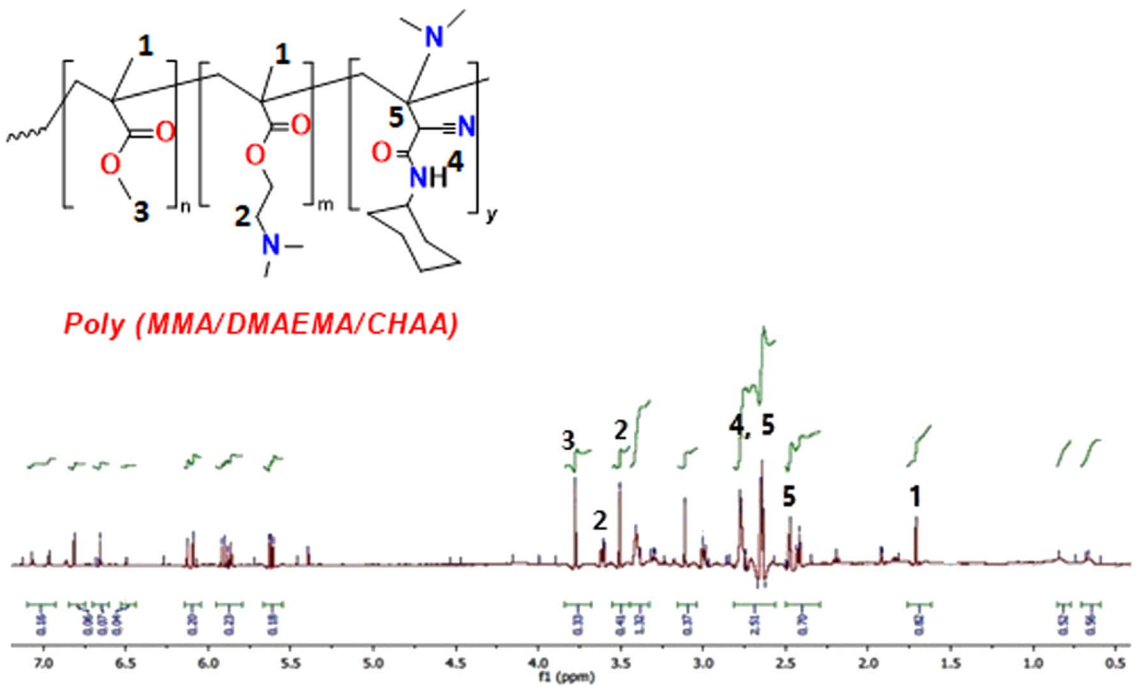

Fig. 5 H^1 NMR of poly(MMA/DMAEMA/CHAA).

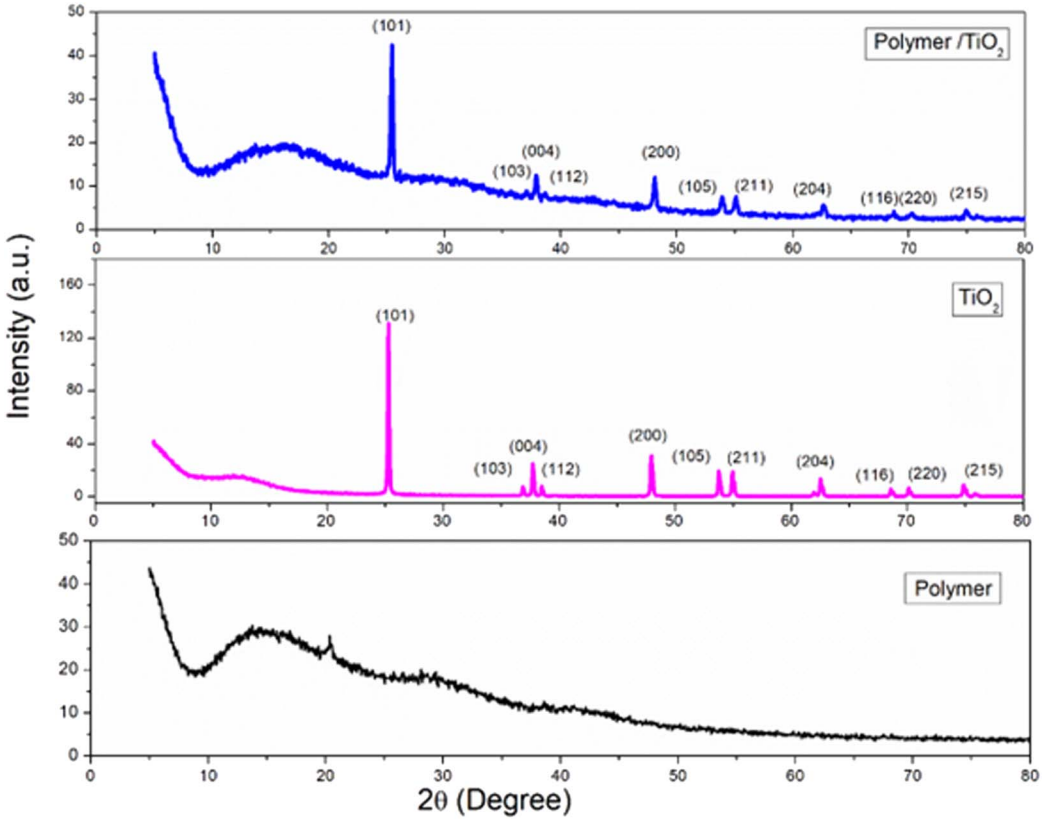

Fig. 6 XRD of pure poly(MMA/DMAEMA/CHAA), TiO_2, and (MMA/DMAEMA/CHAA)-TiO_2.

and 429 cm^{-1} which approved the synthesized TiO_2 nanoparticles.[31–33]

Poly(MMA/DMAEMA/CHAA) was analyzed by FT-IR with wave numbers ranging between 400 and 4000 cm^{-1} as observed in Fig. 4. The broad band centered at 3216 cm^{-1} was assigned to the NH of CHAA. The peak at 1660 cm^{-1} corresponds to the stretching vibration of the carbonyl from CHAA. The peak at 1400 cm^{-1} was caused by the bending vibration of the methyl group in MMA.[34] The peaks at 2940 cm^{-1}, 2190 cm^{-1}, and 1400 cm^{-1} are ascribed to the stretching and bending vibrations of methylene group, respectively.[35] The peaks at 1282 cm^{-1} and 1066 cm^{-1} arise from the vibrational stretching of the methoxy group. The peak at 1066 cm^{-1} belongs to C–N vibrational stretching from DMAEMA (Fig. 4).[36] All these results suggest that poly(MMA/DMAEMA/CHAA) nanospheres have been successfully synthesized.

In poly(MMA/DMAEMA/CHAA)-V_2O_5, the two bands at 1725 and 1660 cm^{-1} in the pure polymer became not tantamount in poly(MMA/DMAEMA/CHAA)-V_2O_5 nanocomposite. The broad two peak at 1400 and 1066 cm^{-1} for pure polymer converted to

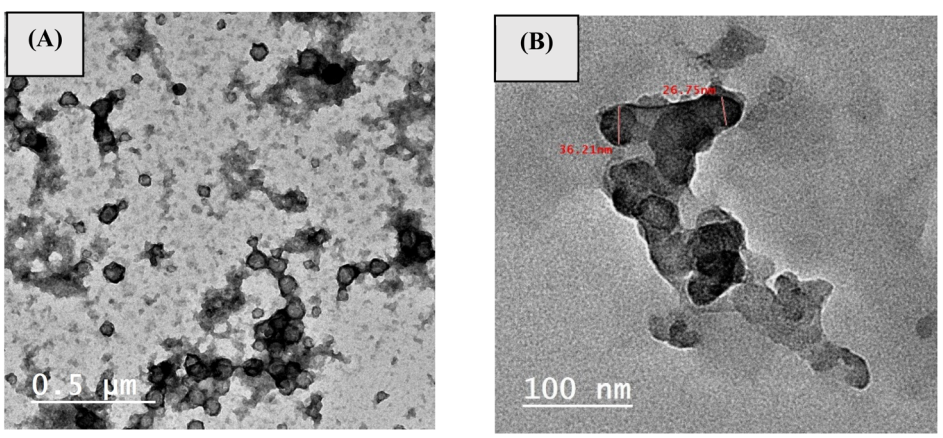

Fig. 7 TEM of (a) poly(MMA/DMAEMA/CHAA) and (b) poly(MMA/DMAEMA/CHAA)-TiO_2.

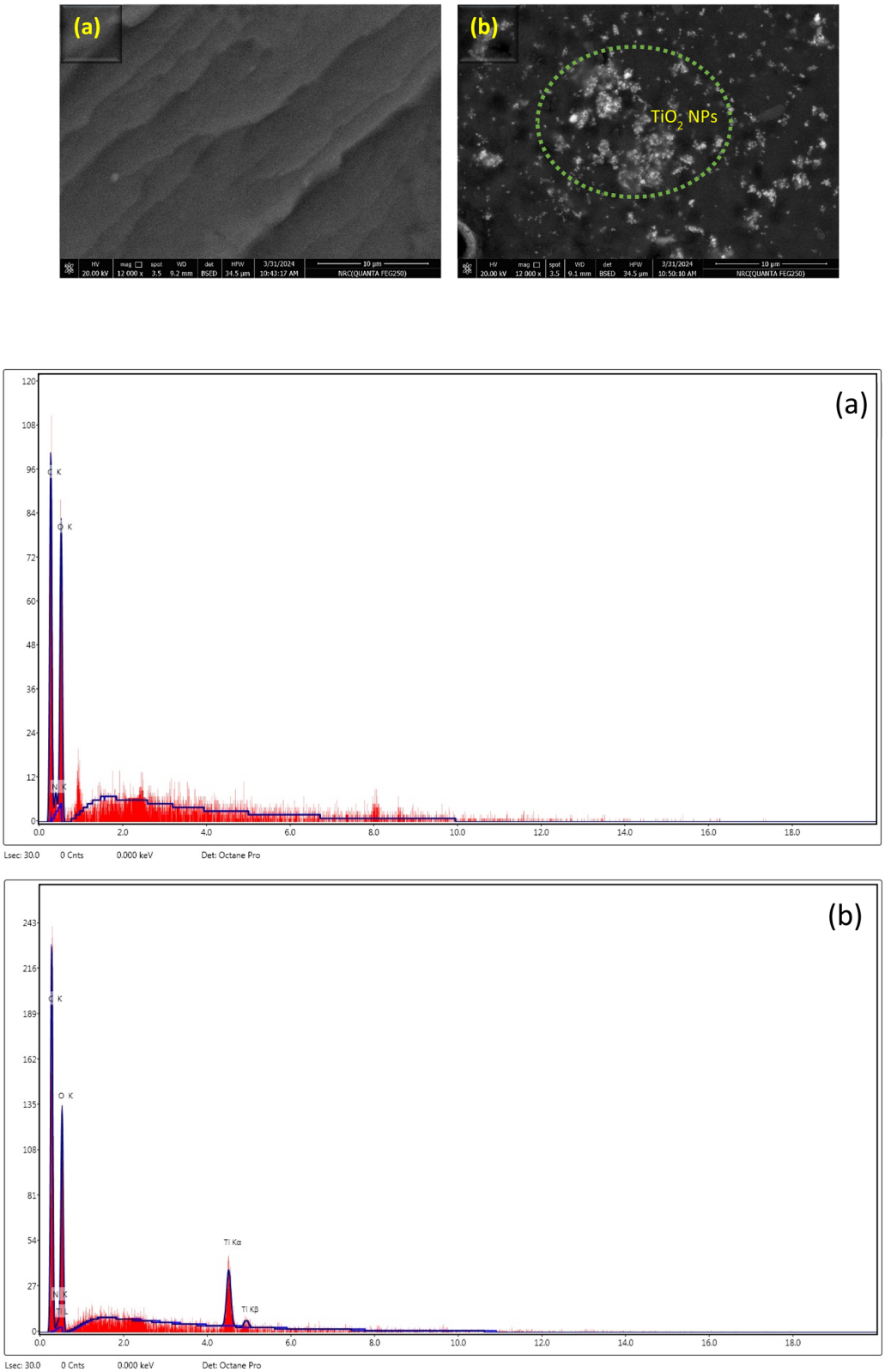

Fig. 8 SEM and EDX of (a) poly(MMA/DMAEMA/CHAA) and (b) poly(MMA/DMAEMA/CHAA)-TiO_2.

sharp peak at polymer-V_2O_5. Furthermore, the one sharp peak at 612 cm^{-1} in poly(MMA/DMAEMA/CHAA) converted to broad peak in the prepared polymeric nanocomposite at 614 cm^{-1} because of the formation of poly(MMA/DMAEMA/CHAA)-V_2O_5. These behaviors indicate the presence of hybrid bonding between polymer matrix and V_2O_5 nanoparticles.[37,38] Moreover,

as shown in Fig. 4, the two equivalent sharp bands at 1725 and 1660 cm^{-1} in the pure polymer became not tantamount in poly(MMA/DMAEMA/CHAA)-TiO_2 nanocomposite. Furthermore, the broad peak at 1440 cm^{-1} in poly(MMA/DMAEMA/CHAA) converted to two peaks in the prepared polymeric nanocomposite at 1445 and 1373 cm^{-1}. The broad peak at 1066 cm^{-1} in a pure polymer converted into sharp peak at 1144 cm^{-1} in poly(MMA/DMAEMA/CHAA)-TiO_2. The other distinctive bands of poly(MMA/DMAEMA/CHAA)-TiO_2 nanocomposite appeared with no change in the wavelength's position with respect to the pure poly(MMA/DMAEMA/CHAA) nanospheres. These behaviors indicate the presence hybrid bonding between TiO_2 nanoparticles and the polymer matrix.[39]

3.2.3. H^1 NMR. The H^1 NMR analysis was utilized to identify the protons of the synthesized poly(MMA/DMAEMA/CHAA). In Fig. 5, the presence of CH_3 and CH_2 in the aliphatic regions (0.56–2.29 ppm) was attributed to the protons of MMA, DMAEMA, and CHAA. The CH_2 of the ester appeared at 4.15 ppm, the CH_2 attached to $N(CH_3)_2$ showed at 3.62 ppm as multiple signals, and the OCH_3 signal was observed at 3.78 ppm. The protons of NH of CHAA were detected at 2.75 ppm.

3.2.4. XRD analysis. The structural characteristics of the synthesized materials were examined using XRD. The XRD patterns of all samples obtained were presented in Fig. 6. To assess the impact of implantation of nanostructures on the matrix of polymeric materials, these nanocomposites were subjected to XRD analysis. The characteristic peaks of TiO_2 nanoparticles in the XRD appeared at 2θ angles of 25.43° (110), 37.0° (103), 37.8° (004), 38.6° (112), 48.0° (200), 53.9° (105), 55.1° (211), 62.6° (204), 68.8° (116), 70.3° (220) and 75.1° (215) which align with the standard spectrum (JCPDS 89-4921).[40,41] The TiO_2 particle sizes ranged from 12 to 22 nm. According to the pure polymer data it contains three peaks signifying a low crystalline structure system, located at around $2\theta = 14.3°$ and a less intense shoulder at $2\theta = 29.3°$ and $2\theta = 41.5°$. This diffractogram pattern exhibited the conventional existence of a semi-crystalline structure and like other findings previously reported in the literature,[42] is mostly atactic, as evidenced by its low crystallinity degree. The poly(MMA/DMAEMA/CHAA)-TiO_2 exhibited the same behavior with a similar peak but with less intensity compared with the pure polymer and TiO_2 nanoparticles individually.

3.3. Morphological analysis

3.3.1. TEM. Fig. 7 showed the TEM images of poly(MMA/DMAEMA/CHAA) and poly(MMA/DMAEMA/CHAA)-MOs nanocomposites, investigating the morphology and size of the produced polymers. As shown in Fig. 7A, pure poly(MMA/DMAEMA/CHAA) was produced in a well-defined nanosphere shape with a particle size of around 45 nm. Furthermore, Fig. 7B showed that the dispersed poly(MMA/DMAEMA/CHAA)-TiO_2 nanocomposite has perfect sphere-shaped morphologies with particle sizes of approximately 75 nm for TiO_2, which consists of dark spheres, proving the embedding of TiO_2. The addition of selenium oxide to the polymeric matrix enhanced the appearance of the composite spheres and made them smoother.

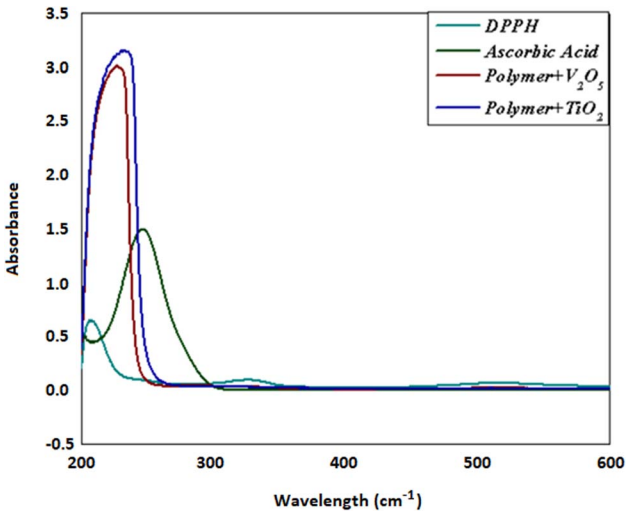

Fig. 9 Typical absorption spectra of 100 μM of the DPPH radical alone and in the presence of a 200 μM concentration of polymer + V_2O_5, polymer + TiO_2 and vitamin C.

3.3.2. SEM and EDX. The morphologies of poly(MMA/DMAEMA/CHAA) and the newly developed poly(MMA/DMAEMA/CHAA)-TiO_2 and poly(MMA/DMAEMA/CHAA)-V_2O_5 were examined using a scanning electron microscope. The surface morphology of pure poly(MMA/DMAEMA/CHAA) displayed smooth layers with a wavy texture as shown in Fig. 8(a). The presence of TiO_2 nanoparticles on the surface of the polymer confirmed the formation of poly(MMA/DMAEMA/CHAA)-TiO_2, as depicted in Fig. 8(b). Similarly, the preparation of the poly(MMA/DMAEMA/CHAA)-V_2O_5 was evidenced through the clear presence of V_2O_5 nano-sheets, as seen in Fig. S1.† Energy-dispersive X-ray spectroscopy measurements were used to quantitatively study the composition of poly(MMA/DMAEMA/CHAA) and poly(MMA/DMAEMA/CHAA)-MO_x nanocomposites. The EDX spectra of pure nanospheres indicated an average composition of 38.89% C, 48.6% O, and 12.51% N. Furthermore, the presence of TiO_2 and V_2O_5 in the nanocomposites was confirmed by the EDX spectra. The analysis revealed that the novel poly(MMA/DMAEMA/CHAA)-TiO_2 had an average composition of 42.48% C, 42.96% O, 9.79% N, and 4.78% Ti (Fig. 8). Additionally, poly(MMA/DMAEMA/CHAA)-V_2O_5 was found to contain 39.92% C, 40.96% O, 11.92% N, and 7.2% V as observed in the EDX spectra. These results indicate the

Table 1 IC_{50} of polymer + V_2O_5 and polymer + TiO_2, respectively for the DPPH radical in methanol

Materials	IC_{50} (μM)
Polymer + V_2O_5	116.98
Polymer + TiO_2	108.42
Ascorbic acid	140.90

successful formation of nanospheres and nanocomposites (Fig. S1†).

3.4. Antioxidant activity

We evaluated the radical scavenging capabilities of the compound's poly(MMA/DMAEMA/CHAA)-V_2O_5 and poly(MMA/DMAEMA/CHAA)-TiO_2 using the 2,2-diphenyl-1-picrylhydrazyl (DPPH) assay in methanol. In this assay, DPPH free radicals undergo a color change from purple to yellow when quenched in the presence of an antioxidant. Typically, the DPPH radical is observed at 517 nm, where the absorption diminishes with the presence of antioxidants, as illustrated in Fig. 9. The graph depicted the percentage inhibition plotted against the concentration of the antioxidant. As indicated in Table 1, both poly(MMA/DMAEMA/CHAA)-V_2O_5 and poly(MMA/DMAEMA/CHAA)-TiO_2 exhibit antioxidant properties. Poly(MMA/DMAEMA/CHAA)-TiO_2 demonstrated the most robust antioxidant effects compared to poly(MMA/DMAEMA/CHAA)-V_2O_5, with a half-maximal inhibitory concentration (IC_{50}) of around 108.42 and 116.98 μM, respectively, comparable to vitamin C ($IC_{50} \sim 140.900$ M). The IC_{50} values suggested that the inclusion of metal oxide on the polymer's surface enhances its radical scavenging abilities against DPPH radicals, as presented in Fig. 9.

3.5. Electrochemical properties study

Cyclic voltammetry (CV) and electrochemical impedance spectroscopy (EIS) techniques were used for characterizing and

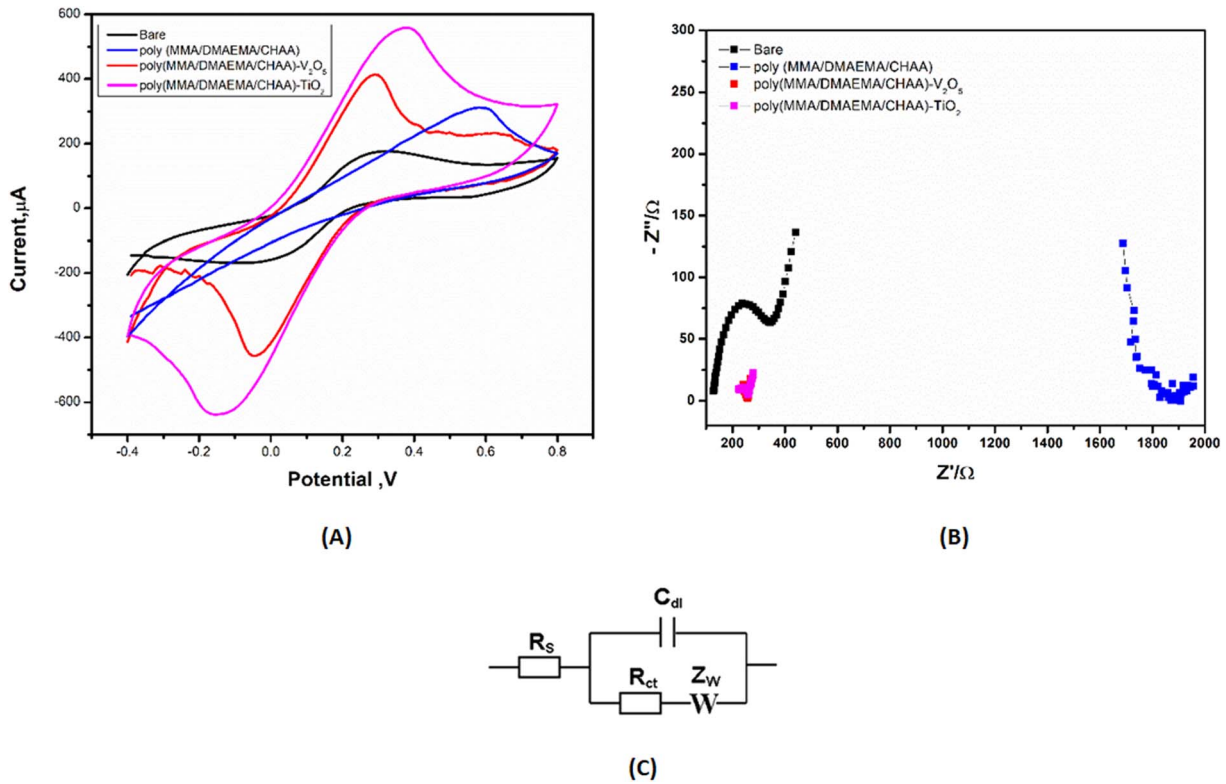

Fig. 10 (A) CV and (B) EIS data for the different poly(MMA/DMAEMA/CHAA)-MOs nanocomposites performance using a mixture solution of 5 mM ferri/ferrocyanide and 0.1 M KCl and scan rate of 50 mV s^{-1}. (C) Fitting circuit.

Table 2 CV and EIS data which measured from the experimental work[a]

Electrode type	I_a (μA)	I_c (μA)	$E_{oxd.}$ (V)	$E_{red.}$ (V)	$E_{1/2}$ (V)	R_s (Ω)	$R_{ct\ (1)}$ (Ω)	W (Ω)	C (μF)
Bare	169	−167	0.35	−0.02	0.165	89.3	560	0.0068	108.1
Poly(MMA/DMAEMA/CHAA)	317		0.51		0.25	96.2	1800	0.0094	83.3
Poly(MMA/DMAEMA/CHAA)-V_2O_5	414	−456.2	0.28	−0.04	0.12	150.2	100	0.0043	306.2
Poly(MMA/DMAEMA/CHAA)-TiO_2	554	−639	0.35	−0.13	0.11	201.3	50	0.0038	374.5

[a] I_a: the anodic current E_{oxd}: the potential of oxidation, I_c: the cathodic current, E_{red}: the potential of reduction, $E_{1/2}$: the half wave potential, R_s: the solution resistance R_{ct}: the charge transfer resistance W: the Warburg resistance, C: the capacitance.

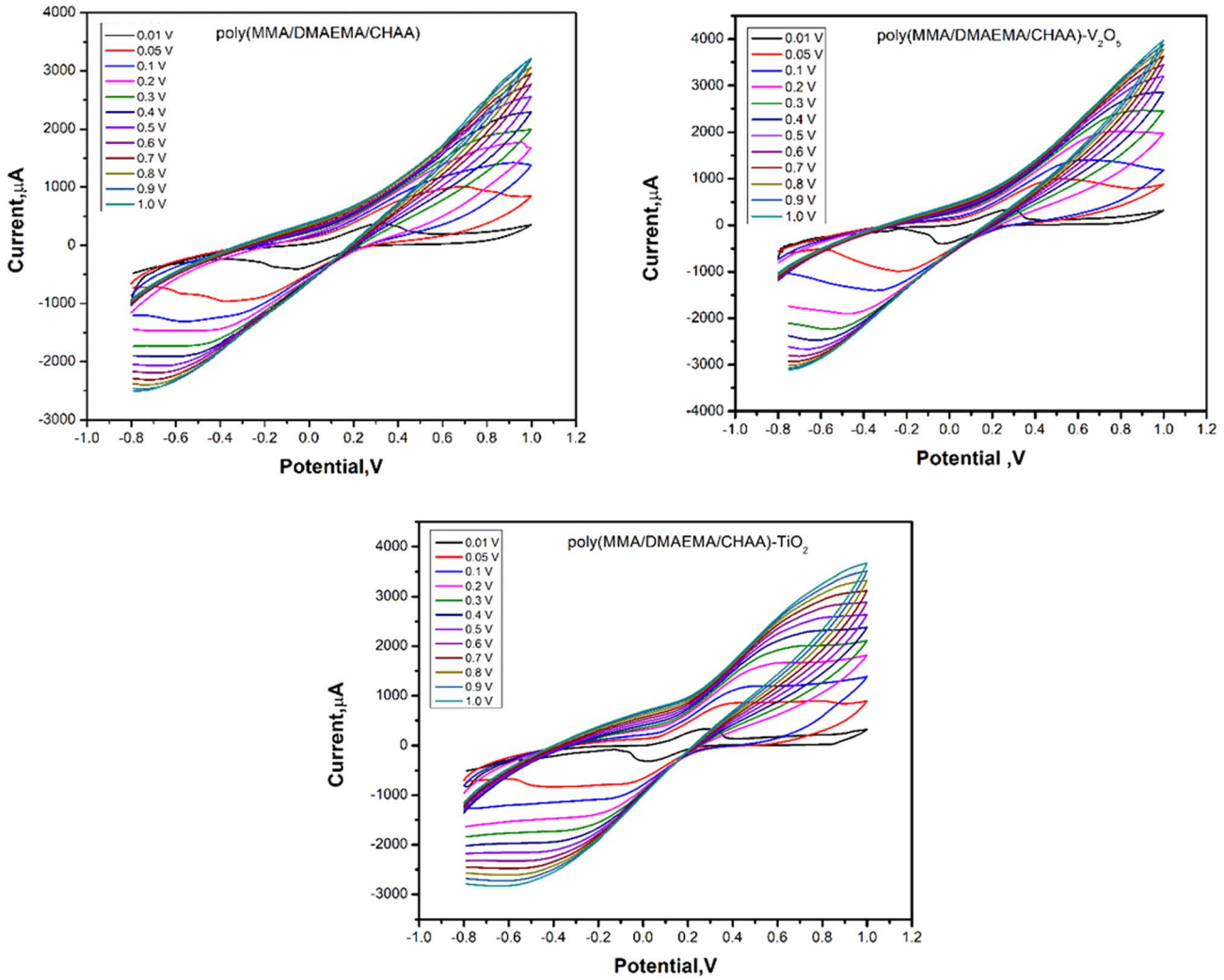

Fig. 11 CVs of different prepared poly(MMA/DMAEMA/CHAA)-MOs nanocomposites at different scan rates.

studying the chemical processes in electrochemical systems. This is allowed for monitoring the performance and stability of synthesized materials using CV and EIS electrochemical methods, as well as properties of charge transfer.[43] A thin film of synthesized materials was modified on the surface of the screen-printed electrode (SPE) and their electrochemical characterization was studied using CV and EIS techniques. The CV results showed a high faradaic current was produced from the fast redox reaction of ferro/ferri cyanide at the poly(MMA/DMAEMA/CHAA)-TiO_2 modified SPE compared to the non-modified SPE (Fig. 10). In parallel with CV measurements, EIS studies were conducted and the Nyquist plot (Fig. 10) of the modified electrode with the poly(MMA/DMAEMA/CHAA)-TiO_2 showed the smallest value of electron charge transfer resistance (Rct) (the circuit used for fitting was shown in Fig. 10) which was consistent with the CV measurements. These studies confirmed the high electrochemical conductivity properties of the poly(-MMA/DMAEMA/CHAA)-TiO_2 modified SPE (Table 2).

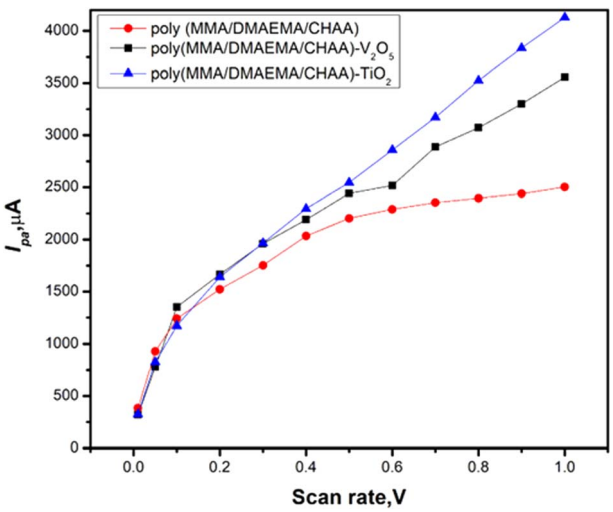

Fig. 12 Cathodic current calibration curves of different poly(MMA/DMAEMA/CHAA)-MOs nanocomposites at different scan rates.

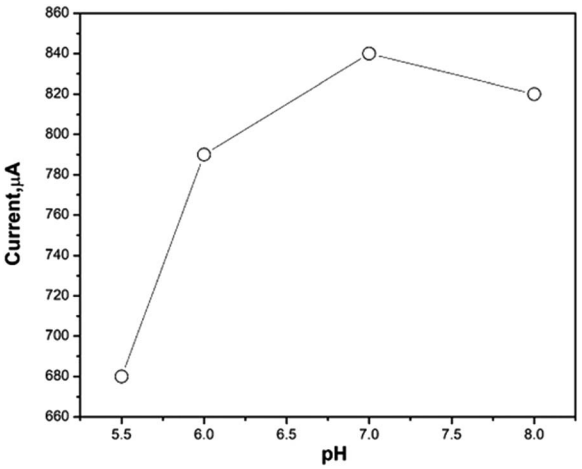

Fig. 13 The pH effect on poly(MMA/DMAEMA/CHAA)-TiO_2 sensor performance towards peroxide oxidation response.

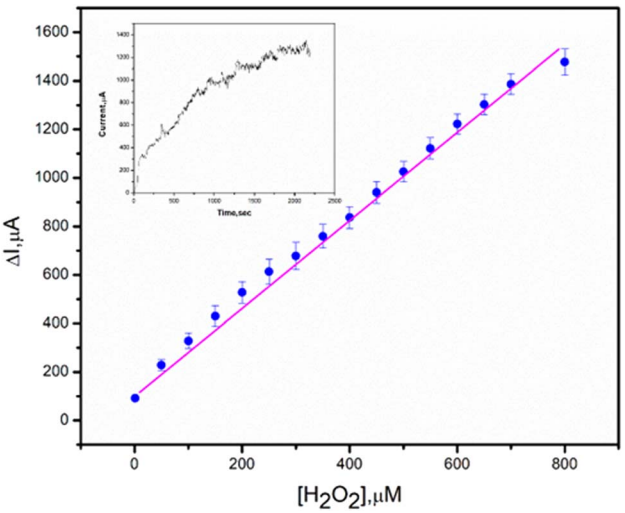

Fig. 15 The corresponding calibration curve of poly(MMA/DMAEMA/CHAA)-TiO_2 modified SPE toward H_2O_2 response.

The effect of scan rate on the cyclic voltammetry of materials modified on SPE was studied over a wide range between 0.01 and 1.0 V (Fig. 11). The calibration curves between current and scan rate (Fig. 12) showed that the cathodic peak current increased as the scan rate increased. This increase in faradaic current confirms the pseudocapacitive properties of the materials. Additionally, during the charge and discharge process, the charge transfer is facilitated by the fast and high faradaic current of redox peaks at the surface of the modified electrodes.

3.6. Poly(MMA/DMAEMA/CHAA)-based MOs platform for H_2O_2 detection

The promising applications of the newly synthesized nanomaterials in biosensors involve the need for fast and direct electron transfer are needed in non-enzymatic sensors for peroxide detection.[44,45] To test this, poly(MMA/DMAEMA/CHAA)-TiO_2 modified SPE was used for peroxide detection by introducing various concentrations of H_2O_2 and observing the resulting increase in current response. The pH of the medium directly affects peroxide oxidation peaks, with different pH values ranging from 5 to 8 being studied. As shown in Fig. 13, the current of peroxide oxidation increased with rising pH up to pH = 7 then decreased. Therefore, a phosphate buffer at pH = 7 was chosen for subsequent experiments.

Eventually, chronoamperometric techniques were used for hydrogen peroxide detection. The newly synthesized materials poly(MMA/DMAEMA/CHAA), poly(MMA/DMAEMA/CHAA)-V_2O_5 and poly(MMA/DMAEMA/CHAA)-TiO_2 modified screen printed electrodes were tested for hydrogen peroxide detection. A specific concentration of hydrogen peroxide was added at fixed time intervals (50 seconds), and the current response was recorded for each concentration. The calibration curves between hydrogen peroxide concentration and current response (Fig. 14) showed a fast and high response for the poly(MMA/DMAEMA/CHAA)-TiO_2 modified SPE, indicating its superior electrocatalytic activity and electron transfer compared to the others. Therefore, the synthesized poly(MMA/DMAEMA/CHAA)-TiO_2 can be utilized as a non-enzymatic sensor for hydrogen peroxide detection. The calibration curve for hydrogen peroxide detection exhibited a linear range response from 1.0 to 800 μM with a detection limit (S/N = 5) of 0.0085 μM (Fig. 15). This confirms that the newly synthesized material poly(MMA/DMAEMA/CHAA)-TiO_2 opens new possibilities for sensor and biosensor constructions.

Comparison between the modified poly(MMA/DMAEMA/CHAA)-TiO_2/SPE as a non-enzymatic sensor toward peroxide detection with the others peroxide sensors in the literature approved that the poly(MMA/DMAEMA/CHAA)-TiO_2/SPE was an excellent nanomaterial for peroxide detection with a wide linear range and low detection limit (Table 3).

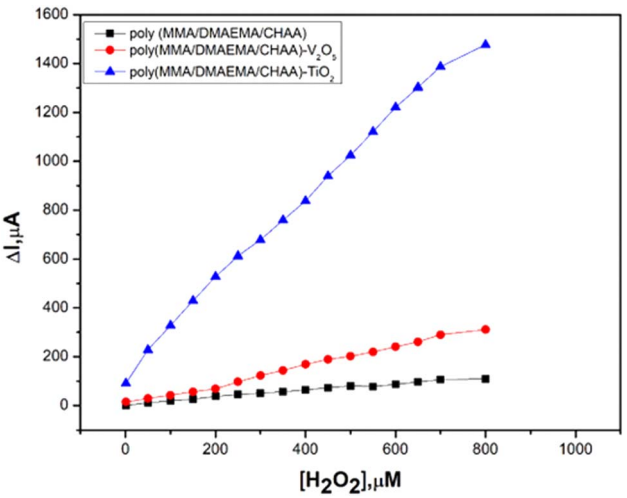

Fig. 14 Amperometry calibration curves of different poly(MMA/DMAEMA/CHAA)-MOs nanocomposites in PBS buffer pH 7.0 and different concentrations of H_2O_2.

Table 3 Comparison of electrochemical response between poly(MMA/DMAEMA/CHAA)-TiO_2 composite *via* different nonenzymatic sensor for peroxide detection[a]

	Sensor performance			
Nanocomposites	LR (μM)	DL (μM)	Synthesis method	References
Pt/rGO-CNT paper electrode	0.1–25	0.01	Sputter deposition	46
Co_3O_4-rGO	15–675	2.4	Hydrothermal	47
$MnCo_2O_3$/CNTs/SPE	0.1–180	0.1	Chemical	13
GO/MnO_2/CNTs	1–210	0.08	Microwave	12
Poly(MMA/DMAEMA/AA)-SeO_2	2.5–750	0.01	Polymerization	16
Poly saccharide/MnO_2	0.2–400	0.04	Chemical	48
Calcium phosphate/$Cu_xFe_{3-x}O_4$ core–shell nanoceramics	2.5–200	0.8	Chemical	49
$BaTi_{0.7}Fe_{0.3}O_3$@$NiFe_2O_4$ (BFT@NFO)	0.1–650	0.01	Chemical	50
Poly(MMA/DMAEMA/CHAA)-TiO_2	1–800	0.0085	Polymerization	This work

[a] LR: linear range DL: detection limit.

4. Conclusions

Poly(MMA/DMAEMA/CHAA) nanocomposites with various synthesized metal oxides (MOs) were successfully produced using a microemulsion polymerization method. FT-IR, ^{1}H NMR, XRD, SEM, EDX, and TEM analyses confirmed the formation of poly(MMA/DMAEMA/CHAA) and its incorporation of MOs in the nanocomposites. When combined with TiO_2 and V_2O_5 nanoparticles, poly(MMA/DMAEMA/CHAA) exhibited excellent current-carrying capacity and electrolyte access, making it an important component in electroactive systems. The newly developed nanocomposite demonstrated superior sensor technology and effectiveness in supercapacitors. Poly(MMA/DMAEMA/CHAA)-MOs nanocomposites were utilized to modify screen-printed electrodes for H_2O_2 detection. Electrochemical results confirmed that these novel poly(MMA/DMAEMA/CHAA)-TiO_2 nanocomposites can effectively detect H_2O_2 in bioanalysis, such as enzyme-based sensors. In conclusion, poly(MMA/DMAEMA/CHAA)-MOs nanocomposites possess unique structural, thermal, morphological, and electrical properties, making them suitable for various applications including catalysis, sensors, biosensors, energy storage, and supercapacitors.

Data availability

Authors confirm that the data supporting the findings of this study are available within the article.

Conflicts of interest

The authors declare that none of the work reported in this study has been influenced by any known financial or personal relationships.

Acknowledgements

Under the auspices of its internal project (with ID: 13020103), National Research Centre in Giza, Egypt has provided financial assistance for this work.

References

1 S. Cichosz, A. Masek and M. Zaborski, Polymer-based sensors: A review, *Polym. Test.*, 2018, **67**, 342–348.
2 M. S. Hashem, A. M. Fahim and F. M. Helaly, Designing a green poly (β-amino ester) for the delivery of nicotinamide drugs with biological activities and conducting a DFT investigation, *RSC Adv.*, 2024, **14**, 5499–5513.
3 M. A. Abd El-Ghaffar, K. S. Atia and M. S. Hashem, Synthesis and characterization of binary copolymers of methyl methacrylate with glycidyl methacrylate and 2-hydroxy ethyl methacrylate as carriers for cellulase, *J. Appl. Polym. Sci.*, 2010, **117**, 629–638.
4 H. S. Magar, E. E. Abu-El Magd, R. Y. A. Hassan and A. M. Fahim, Rapid impedimetric detection of cadmium ions using Nanocellulose/ligand/nanocomposite (CNT/Co_3O_4), *Microchem. J.*, 2022, **182**, 107885.
5 G. Alberti, C. Zanoni, V. Losi, L. R. Magnaghi and R. Biesuz, Current Trends in Polymer Based Sensors, *Chemosensors*, 2021, **9**, 108.
6 G. G. Carbone, A. Serra, A. Buccolieri and D. Manno, A silver nanoparticle-poly(methyl methacrylate) based colorimetric sensor for the detection of hydrogen peroxide, *Heliyon*, 2019, **5**, e02887.
7 M. Shamsipur, Z. Karimi and M. A. Tabrizi, A highly sensitive hydrogen peroxide sensor based on (Ag–Au NPs)/poly[o-phenylenediamine] modified glassy carbon electrode, *Mater. Sci. Eng., C*, 2015, **56**, 426–431.
8 A. Teniou, I. A. Madi, R. Mouhoub, J. L. Marty and A. Rhouati, One-Step Chemiluminescent Assay for Hydrogen Peroxide Analysis in Water, *Chemosensors*, 2023, **11**, 455.
9 X. Wang, A. Jiang, T. Houa and F. Li, A sensitive and versatile "signal-on" electrochemical aptasensor based on a triple-helix molecular switch, *Analyst*, 2014, **139**, 6272–6278.
10 H. S. Magar, M. E. Ghica, M. N. Abbas and C. M. A. Brett, A novel sensitive amperometric choline biosensor based on

multiwalled carbon nanotubes and gold nanoparticles, *Talanta*, 2017, **167**, 462–469.

11 H. S. Magar, M. E. Ghica, M. N. Abbas and C. M. A. Brett, Highly Sensitive Choline Oxidase Enzyme Inhibition Biosensor for Lead Ions Based on Multiwalled Carbon Nanotube Modified Glassy Carbon Electrodes, *Electroanalysis*, 2017, **29**, 1741–1748.

12 M. N. Abbas and H. S. Magar, Highly sensitive and selective solid-contact calcium sensor based on Schiff base of benzil with 3-aminosalycilic acid covalently attached to polyacrylic acid amide for health care, *J. Solid State Electrochem.*, 2018, **22**, 181–192.

13 G. Abd El-Fatah, H. S. Magar, R. Y. A. Hassan, R. Mahmoud, A. A. Farghali and M. E. M. Hassouna, A novel gallium oxide nanoparticles-based sensor for the simultaneous electrochemical detection of Pb^{2+}, Cd^{2+} and Hg^{2+} ions in real water samples, *Sci. Rep.*, 2022, **12**, 20181.

14 M. S. Hashem, H. S. Magar, A. M. Fahim and R. A. Sobh, Antimicrobial, antioxidant, mechanistic, docking simulation, and electrochemical studies for grafting polymerization of novel sulphonated gelatin derived from chicken feet, *Mater. Chem. Phys.*, 2023, **310**, 128474.

15 L. D. Chakkarapani, S. Arumugam and M. Brandl, Simultaneous electrochemical detection of L-dopa and hydrogen peroxide by poly (amido amine) dendrimer/poly (neutral red) modified sensor, *J. Food Compos. Anal.*, 2024, **126**, 105847.

16 H. S. Magar, M. S. Hashem and R. A. Sobh, Design of metal oxide nanoparticles-embedded polymeric nanocomposites for hydrogen peroxide chronoamperometric sensor, *J. Polym. Compos.*, 2024, **45**, 3653–3665.

17 B. Haghighi and M. Amouzadeh Tabrizi, Direct electron transfer from glucose oxidase immobilized on an overoxidized polypyrrole film decorated with Au nanoparticles, *Colloids Surf., B*, 2013, **103**, 566–571.

18 R. A. Sobh, H. S. Magar, A. M. Fahim and M. S. Hashem, Construction, molecular docking simulation and evaluation of electrochemical properties of polymeric nanospheres comprising novel synthesized monomer via green microemulsion polymerization, *Polym. Adv. Technol.*, 2024, **35**, e6248.

19 P. Ghosh, T. Das and M. Das, Evaluation of poly (acrylates) and their copolymer as viscosity modifiers, *Res. J. Chem. Sci.*, 2011, **1**, 18–25.

20 P. Ghosh, T. Das and D. Nandi, Synthesis characterization and viscosity studies of homopolymer of methyl methacrylate and copolymer of methyl methacrylate and styrene, *J. Solution Chem.*, 2011, **40**, 67–78.

21 P. Ghosh, T. Das, D. Nandi, G. Karmakar and A. Mandal, Synthesis and characterization of biodegradable polymer – used as a pour point depressant for lubricating oil, *Int. J. Polym. Mater.*, 2010, **59**, 1008–1017.

22 P. Ghosh, M. Das and T. Das, Synthesis, characterization and viscosity studies of acrylate based homo and copolymer, *Res. J. Chem. Environ.*, 2010, **14**, 26–31.

23 M. S. Blois, Antioxidant Determinations by the Use of a Stable Free Radical, *Nature*, 1958, **181**, 1199–1200.

24 M. K. Darwish, M. S. Said, R. A. Sobh and A. A. Abdel-khalek, Tailoring Nano Copolymer/CNTs Composite and its Application in Drug Delivery, *Egypt. J. Chem.*, 2021, **64**, 3335.

25 G. Abdel-Maksoud, R. A. Sobh and A. Tarek, Evaluation of MMI/acrylate nanocomposite with hydroxyapatite as a novel paste for gap filling of archaeological bones, *J. Cult. Herit.*, 2022, **57**, 194.

26 A. Moustafa, R. Sobh, A. Rabie, H. Nasr and M. Ayoub, Differential microemulsion polymerization as a new root for entrapment of drugs, *J. Appl. Polym. Sci.*, 2013, **127**, 4634.

27 A. Moustafa, R. Sobh, A. Rabie, H. Nasr and M. Ayoub, Synthesis and in vitro release of guest drugs-loaded copolymer nanospheres MMA/HEMA via differential microemulsion polymerization, *J. Appl. Polym. Sci.*, 2013, **129**, 853.

28 C. D. Jadhav, B. Pandit, S. S. Karade, B. R. Sankapal and P. G. Chavan, Enhanced field emission properties of V_2O_5/MWCNTs nanocomposite, *Appl. Phys. A: Mater. Sci. Process.*, 2018, **124**, 794.

29 K. M. Shafeeq, V. P. Athira, C. H. Raj Kishor and P. M. Aneesh, Structural and optical properties of V_2O_5 nanostructures grown by thermal decomposition technique, *Appl. Phys. A: Mater. Sci. Process.*, 2020, **126**, 58.

30 M. Farahmandjou and N. Abaeiyan, Chemical synthesis of vanadium oxide (V_2O_5) nanoparticles prepared by sodium metavanadate, *J. Nanomed. Res.*, 2017, **5**, 1–6.

31 M. Irfan, R. Nawaz, J. A. Khan, H. Ullah, T. Haneef, S. Legutko, S. Rahman, J. Józwik, M. A. Alsaiar, M. K. A. Khan, S. N. F. Mursal, F. S. AlKahtani, O. Alshorman and A. A. J. Ghanim, Synthesis and Characterization of Manganese-Modified Black TiO_2 Nanoparticles and Their Performance Evaluation for the Photodegradation of Phenolic Compounds from Wastewater, *Materials*, 2021, **14**, 7422.

32 N. Lertthanaphol, N. Pienutsa, K. Chusri, T. Sornsuchat, P. Chanthara, P. Seeharaj, P. Kim-Lohsoontorn and S. Srinives, One-Step Hydrothermal Synthesis of Precious Metal-Doped Titanium Dioxide– Graphene Oxide Composites for Photocatalytic Conversion of CO_2 to Ethanol, *ACS Omega*, 2021, **6**, 35769–35779.

33 M. R. A. Abada, S. F. Shayesteha and H. F. Shayesteh, Effect of Synthesis Conditions on the Structural, Photocatalic, and Self-Cleaning Properties of TiO_2 Nanoparticles, *Phys. Solid State*, 2020, **62**, 120–130.

34 W. Zou, Y. Huang, J. Luo, J. Liu and C. Zhao, Poly (methyl methacrylate–acrylic acid–vinyl pyrrolidone) terpolymer modified polyethersulfone hollow fiber membrane with pH sensitivity and protein antifouling property, *J. Membr. Sci.*, 2010, **358**, 76.

35 P. Singhal, P. Mazumdar and S. Rattan, One pot synthesis of free standing highly conductive polymer nanocomposite films: Towards rapid BTX vapor sensor, *Polym. Eng. Sci.*, 2018, **58**, 1074.

36 F. Guo, Q. Zhang, W. Wang, H. Zhang and J. Sun, Preparation of pH-responsive Fe_3O_4/Poly (acrylic acid-stat-methyl methacrylate-block-(2-dimethylamino) ethyl methacrylate) magnetic composite microspheres and its

application in controlled release of drug, *Mater. Sci. Eng., C*, 2011, **31**, 938.

37 S. Roy, S. Mishra, P. Yogi, S. K. Saxena, V. Mishra, P. R. Sagdeo and R. Kumar, Polypyrrole–vanadium oxide nanocomposite: polymer dominates crystallanity and oxide dominates conductivity, *Appl. Phys. A: Mater. Sci. Process.*, 2018, **124**, 53.

38 P. Wang, Y. Zhang, Z. Feng, Y. Liu and C. Meng, A dual-polymer strategy boosts hydrated vanadium oxide for ammonium-ion storage, *J. Colloid Interface Sci.*, 2022, **606**, 1322–1332.

39 O. A. Ryabkova, E. V. Salomatina, E. A. Zakharychev, R. R. Shvarev and L. A. Smirnova, Properties of poly(titanium oxide)-containing polymeric materials exhibiting UV-induced superhydrophilicity under simulated climate test conditions, *Results Eng.*, 2022, **15**, 100525.

40 T. Homann, T. Bredow and K. Jug, Adsorption of small molecules on the anatase (100) surface, *Surf. Sci.*, 2004, **555**, 135–144.

41 S. El-Sherbiny, F. Morsy, M. Samir and O. A. Fouad, Synthesis, characterization, and application of TiO_2 nanopowders as special paper coating pigment, *Appl. Nanosci.*, 2013, **4**, 305–313.

42 R. C. de Azevedo Gonçalves Mota, E. O. da Silva and L. R. de Menezes, Effect of the Addiction of Metal Oxide Nanoparticles on the Physical, Chemical and Thermal Properties of PVA Based Nanocomposites, *Mater. Sci. Appl.*, 2018, **9**, 473–488.

43 H. S. Magar, R. Y. A. Hassan and M. N. Abbas, Non-enzymatic disposable electrochemical sensors based on CuO/Co_3O_4@MWCNTs nanocomposite modified screen-printed electrode for the direct determination of urea, *Sci. Rep.*, 2023, **13**, 2034.

44 H. S. Magar, M. N. Abbas, M. Ben Ali and M. A. Ahmed, Picomolar-sensitive impedimetric sensor for salivary calcium analysis at POC based on SAM of Schiff base–modified gold electrode, *J. Solid State Electrochem.*, 2020, **24**, 723–737.

45 H. S. Magar, P. K. Brahman and R. Y. A. Hassan, Disposable impedimetric nano-immunochips for the early and rapid diagnosis of Vitamin-D deficiency, *Biosens. Bioelectron.: X*, 2022, **10**, 100124.

46 Y. Sun, K. He, Z. Zhang, A. Zhou and H. Duan, Real-time electrochemical detection of hydrogen peroxide secretion in live cells by Pt nanoparticles decorated graphene–carbon nanotube hybrid paper electrode, *Biosens. Bioelectron.*, 2015, **68**, 358.

47 L. Kong, Interconnected 1D Co_3O_4 nanowires on reduced graphene oxide for enzymeless H_2O_2 detection, *Nano Res.*, 2015, **8**, 469.

48 H. S. Tohamy and H. S. Magar, A Flexible, Low-Cost, Disposable Non-Enzymatic Electrochemical Sensor Based on MnO2/Cellulose Nanostructure, *ECS J. Solid State Sci. Technol.*, 2022, **11**, 127003.

49 A. Elzwawy, A. M. Mansour, H. S. Magar, A. B. Abou Hammad, R. Y. A. Hassan and A. M. El Nahrawy, Exploring the structural and electrochemical sensing of wide bandgap calcium phosphate/$CuxFe_3$-xO_4 core-shell nanoceramics for H_2O_2 detection, *Mater. Today Commun.*, 2022, **33**, 104574.

50 A. B. Abou Hammad, H. S. Magar, A. M. Mansour, R. Y. A. Hassan and A. M. El Nahrawy, Construction and characterization of nano-oval $BaTi_{0.7}Fe_{0.3}O_3$@$NiFe_2O_4$ nanocomposites as an effective platform for the determination of H_2O_2, *Sci. Rep.*, 2023, **13**, 9048.